

# Proposal for valleytronic materials: ferrovalley metal and valley gapless semiconductor

San-Dong Guo<sup>1</sup>, Yu-Ling Tao<sup>1</sup>, Guang-Zhao Wang<sup>2</sup>, Shaobo Chen<sup>3</sup> and Yee Sin Ang<sup>4</sup>

<sup>1</sup>*School of Electronic Engineering, Xi'an University of Posts and Telecommunications, Xi'an 710121, China*

<sup>2</sup>*Key Laboratory of Extraordinary Bond Engineering and Advanced Materials Technology of Chongqing, School of Electronic Information Engineering, Yangtze Normal University, Chongqing 408100, China*

<sup>3</sup>*College of Electronic and Information Engineering,*

*Anshun University, Anshun 561000, People's Republic of China and*

<sup>4</sup>*Science, Mathematics and Technology (SMT), Singapore University of Technology and Design (SUTD), 8 Somapah Road, Singapore 487372, Singapore*

Valleytronic materials can provide new degrees of freedom to future electronic devices. In this work, the concepts of the ferrovalley metal (FVM) and valley gapless semiconductor (VGS) are proposed, which can be achieved in valleytronic bilayer systems by electric-field tuning, where the interaction between out-of-plane ferroelectricity and A-type antiferromagnetism can induce layer-polarized anomalous valley Hall (LP-AVH) effect. The K and -K valleys of FVM are both metallic, and electron and hole carriers simultaneously exist. In the extreme case, the FVM can become VGS by analogizing spin gapless semiconductor (SGS). Moreover, it is proposed that the valley splitting enhancement and valley polarization reversal can be achieved by electric field in valleytronic bilayer systems. Taking the bilayer RuBr<sub>2</sub> as an example, our proposal is confirmed by the first-principle calculations. The FVM and VGS can be achieved in bilayer RuBr<sub>2</sub> by applying electric field. With appropriate electric field range, increasing electric field can enhance valley splitting, and the valley polarization can be reversed by flipping electric field direction. To effectively tune valley properties by electric field in bilayer systems, the parent monolayer should possess out-of-plane magnetization, and have large valley splitting. Our results shed light on the possible role of electric field in tuning valleytronic bilayer systems, and provide a way to design the ferrovalley-related material by electric field.

Keywords: Valleytronics, Electric field, Bilayer

Email:sandongyuwang@163.com

## I. INTRODUCTION

Manipulating different degrees of freedom of electrons plays a key role in building modern electronic devices. The valley pseudospin is one of the emerging degrees of freedom beyond charge and spin of carriers<sup>1,2</sup>. In crystalline solids, valley is characterized by a local energy extreme for both the conduction or valence band. For many MoS<sub>2</sub>-like monolayers, their conduction band minimum (CBM) and valence band maximum (VBM) are located in two inequivalent momenta -K and K, which constitute a binary valley index<sup>1,3-9</sup>. The intensive efforts have been made to manipulate the valley pseudospin, and a well-known field is established and called valleytronics<sup>10</sup>. The main challenge for valleytronics lies in inducing valley polarization. For systems with time-reversal symmetry, the optical pumping, magnetic field, magnetic substrates and magnetic doping have been proposed to generate valley-polarized states<sup>3-9,11,12</sup>. However, these methods have some disadvantages. The magnetic substrates and magnetic doping destroy intrinsic energy band structures and crystal structures. The optical pumping and magnetic field limit the generation of purely valley-polarized states. The concepts of ferrovalley semiconductor (FVS) [Figure 1 (a)] and half-valley metal (HVM) [Figure 1 (b)] with intrinsic spontaneous valley polarization have been proposed<sup>13,14</sup>, which have been predicted in many two-dimensional (2D) ferromagnets<sup>15-28</sup>. Recently, we have proposed possible electronic state quasi-half-valley-metal (QHVM) [Figure 1 (c)], which contains electron

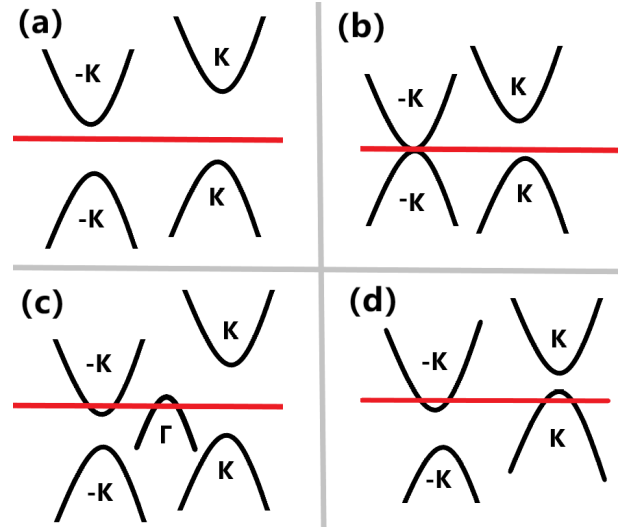


FIG. 1. (Color online) Schematic diagrams of energy bands of ferrovalley semiconductor (a), half-valley-metal (b), quasi-half-valley-metal (c) and ferrovalley metal (d). The horizontal red lines mean Fermi level.

and hole carriers with only a type of carriers being valley polarized<sup>29</sup>.

In analogy to ferromagnetic metal in spintronics, we propose the concept of ferrovalley metal (FVM) [Figure 1 (d)], where the K and -K valleys are both metallic. For FVM, electron and hole carriers simultaneously exist, and the Fermi level slightly touches -K and K valleys

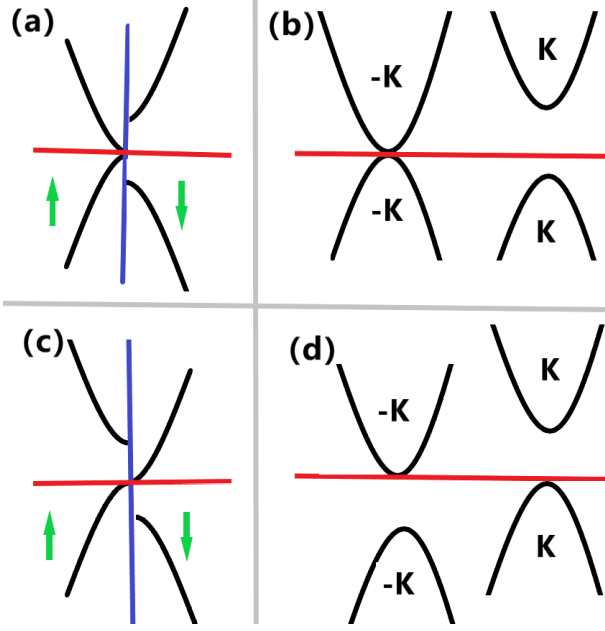


FIG. 2. (Color online) Schematic diagram of the analogy between spin gapless semiconductor (a, c) and valley gapless semiconductor (b, d). The spin-up/spin-dn is equivalent to -K/K valley. The green arrows mean spin, and the horizontal red lines mean Fermi level.

(CBM and VBM). The concept of the spin gapless semiconductor (SGS) [Figure 2 (a) and (c)], where both electron and hole can be fully spin polarized, has been proposed in spintronics<sup>30</sup>. By analogizing SGS, the concept of the valley gapless semiconductor (VGS) is proposed in this work. There are two possible band structure configurations with valley gapless features as illustrated in Figure 2 (b) and (d). For the first case [Figure 2 (b)], one valley is gapless, while the other valley is semiconducting. In fact, the first case is HVM, which has been proposed in ref<sup>14</sup>. In the second case [Figure 2 (d)], there is a gap between the conduction and valence bands for both the -K and K valleys, while there is no gap between -K valley in the valence band and K valley in the conduction band (or K valley in the valence band and -K valley in the conduction band), which is named as VGS-2. The second case is the extreme case of FVM, where the Fermi level exactly touches -K and K valleys (CBM and VBM). The schematic diagrams of the analogy between SGS and VGS are plotted in Figure 2.

It is difficult to find these materials of FVM and VGS-2 in simple compounds. Recently, layer-polarized anomalous Hall effect in valleytronic van der Waals bilayers by interlayer sliding has been proposed from 2D systems with spontaneous valley polarization<sup>31</sup>. The interaction between the out-of-plane ferroelectricity and A-type antiferromagnetism allows the realization of layer-polarized anomalous valley Hall (LP-AVH) effect. The ferroelectric switching can induce reversed sign change of valley polarization. The out-of-plane ferroelectricity polarization

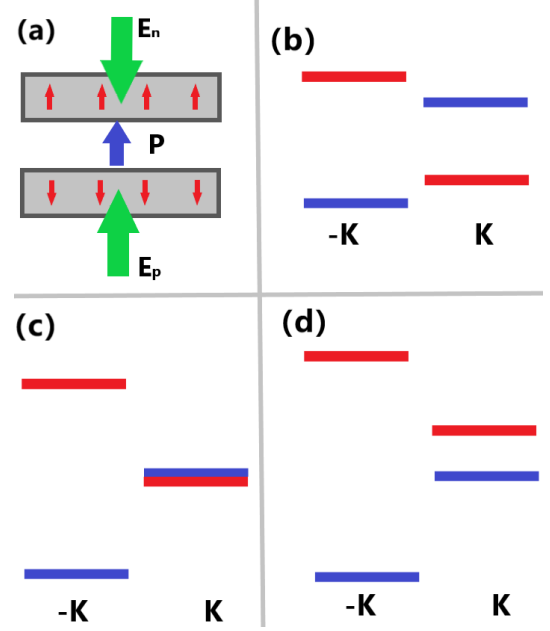


FIG. 3. (Color online)(a): The schematic diagram of a bilayer lattice with AB pattern, and the red, blue and green arrows represents spin, electric polarization  $P$  and external electric field  $E_p$  (positive  $z$  direction) and  $E_n$  (negative  $z$  direction). The energy level of -K and K valleys without (b) and with external electric field  $E_p = E_p^c$  (c) and  $E_p > E_p^c$  (d). The red (blue) energy levels are from dn-layer (up-layer).

is equivalent to an electric field<sup>32</sup>, so an external electric field can be used to tune layer valley polarization, which provides possibility to achieve FVM and VGS-2.

As shown in Figure 3 (a), a AB-stacked bilayer lattice from a 2D system with main spontaneous valley polarization in the conduction bands ( $d_{x^2-y^2} + d_{xy}$ -dominated orbitals) has positive electric polarization, and layer spontaneous valley polarization can be observed (Figure 3 (b)). Without out-of-plane electric polarization, the energies of -K and K valleys from different layer are coincident. By applying an out-of-plane electric polarization or external electric field penetrating from dn-layer to up-layer (defined as the positive field) (see Figure 3 (a)), the energy band from dn-layer is shifted toward high energy with respect to one of up-layer, which leads to spontaneous valley polarization. As long as the valley splitting of pristine monolayer between -K and K valleys is big enough (This is larger than one caused by out-of-plane electric polarization in bilayer system.), the -K and K valleys of bilayer system are from different layer (see Figure 3 (b)). When increasing positive external electric field  $E_p$ , the energy levels at K valley from different layers will coincide at a critical electric field  $E_p^c$  (see Figure 3 (c)). When continuing to increase  $E_p$ , the -K and K valleys of bilayer system are from the same up-layer (see Figure 3 (d)). When an appropriate positive external electric field ( $E_p < E_p^c$ ) is applied, the spontaneous valley polarization (valley splitting) should be

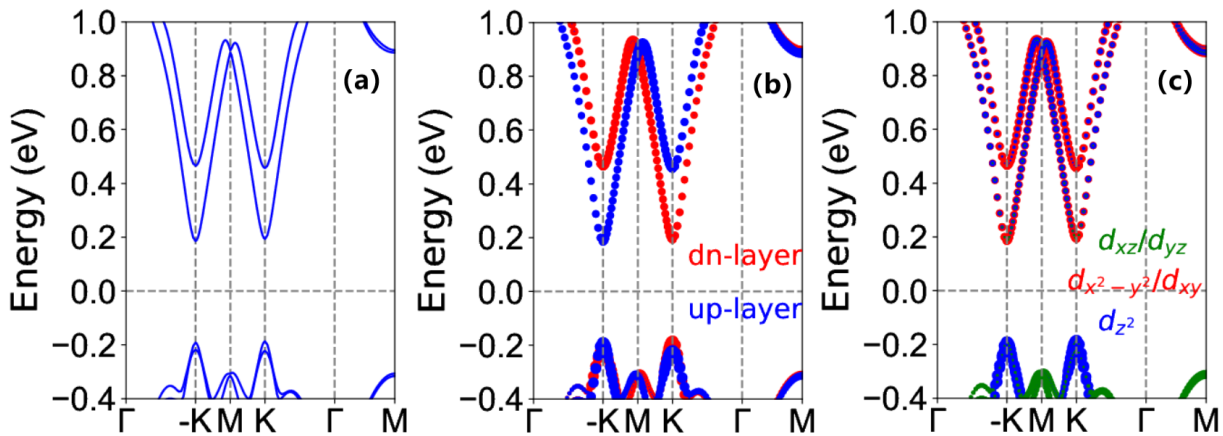


FIG. 4. (Color online)(a): The band structures of AB-stacked bilayer RuBr<sub>2</sub>, including layer- (b) and Ru-*d*-orbital (c) characters energy band structures.

enhanced. However, when the external electric field is reversed (An appropriate negative external electric field ( $E_n$ ) is applied.), the sign of valley polarization can also be reversed (The -K and K valleys along the levels from up-layer and dn-layer exchange each other.). The above analysis also apply to the valence bands ( $d_{z^2}$ -dominated orbitals) with small spontaneous valley polarization, and the critical electric field  $E_p^v$  is very small. By applying an out-of-plane external electric field penetrating from dn-layer to up-layer, the energy band from dn-layer is shifted toward high energy with respect to one of up-layer, which can realize VGS-2 and FVM.

Here, a concrete example of bilayer RuBr<sub>2</sub> is used to illustrate our idea. Calculated results show that increasing electric field indeed can enhance valley splitting in bilayer RuBr<sub>2</sub>, and make K and -K valleys be from the same layer. The possible electronic states VGS-2 and FVM can be achieved in bilayer RuBr<sub>2</sub> caused by electric filed. Our findings can be extended to other valleytronic bilayers, and tune their valley properties by electric field.

The rest of the paper is organized as follows. In the next section, we shall give our computational details and methods. In the next section, we shall present crystal structure, electronic structures and electric field effects on physical properties of bilayer RuBr<sub>2</sub>. Finally, we shall give our discussion and conclusion.

## II. COMPUTATIONAL DETAIL

Within density-functional theory (DFT)<sup>33</sup>, the spin-polarized calculations are carried out by employing the projected augmented wave method, as implemented in VASP code<sup>34-36</sup>. We use the generalized gradient approximation of Perdew-Burke-Ernzerhof (PBE-GGA)<sup>37</sup> as exchange-correlation functional. To consider on-site Coulomb correlation of Ru atoms, the GGA+*U* method in terms of the on-site Coulomb interaction of  $U = 2.5$  eV<sup>26,27</sup> is used within the rotationally invariant approach

proposed by Dudarev et al<sup>38</sup>. To attain accurate results, we use the energy cut-off of 500 eV, total energy convergence criterion of  $10^{-7}$  eV and force convergence criteria of less than  $0.001$  eV.Å<sup>-1</sup> on each atom. To avoid the interactions between the neighboring slabs, a vacuum space of more than 20 Å is used. The dispersion-corrected DFT-D3 method<sup>39</sup> is adopted to describe the van der Waals interactions between individual layers. The  $\Gamma$ -centered  $18 \times 18 \times 1$  k-point meshes in the Brillouin zone (BZ) are used for structure optimization and electronic structures calculations. The spin-orbital coupling (SOC) effect is explicitly included to investigate magnetic anisotropy energy (MAE) and electronic properties of bilayer RuBr<sub>2</sub>. The Berry curvatures are calculated directly from wave functions based on Fukui's method<sup>40</sup> by using VASPBERRY code<sup>41,42</sup>. Under an electric field, the atomic positions are relaxed. To easily meet energy convergence criterion, the parameter DIPOL=0.5 0.5 0.5 is set, and the convergent charge density under small electric field gradually feeds to the calculations with large electric field.

## III. ELECTRONIC STRUCTURES

The LP-AVH effect has been demonstrated in a series of valleytronic materials, such as VSi<sub>2</sub>P<sub>4</sub>, VSi<sub>2</sub>N<sub>4</sub>, FeCl<sub>2</sub>, RuBr<sub>2</sub> and VClBr<sup>31</sup>. To clearly demonstrate our previous analysis of electric field effects on valley polarization in valleytronic bilayers (Figure 3), the parent monolayer should have large valley splitting. The previous works show that RuBr<sub>2</sub> has very large valley splitting in the conduction bands or valence bands, which depends on the electronic correlation strength or strain<sup>26,27</sup>. Therefore, the RuBr<sub>2</sub> monolayer is used to validate our proposal.

The RuBr<sub>2</sub> monolayer consists Br-Ru-Br sandwich layer, and shares the same crystal structure with MoS<sub>2</sub>. It has a hexagonal lattice with the space group  $P\bar{6}m2$ , and its inversion symmetry is broken, which along with

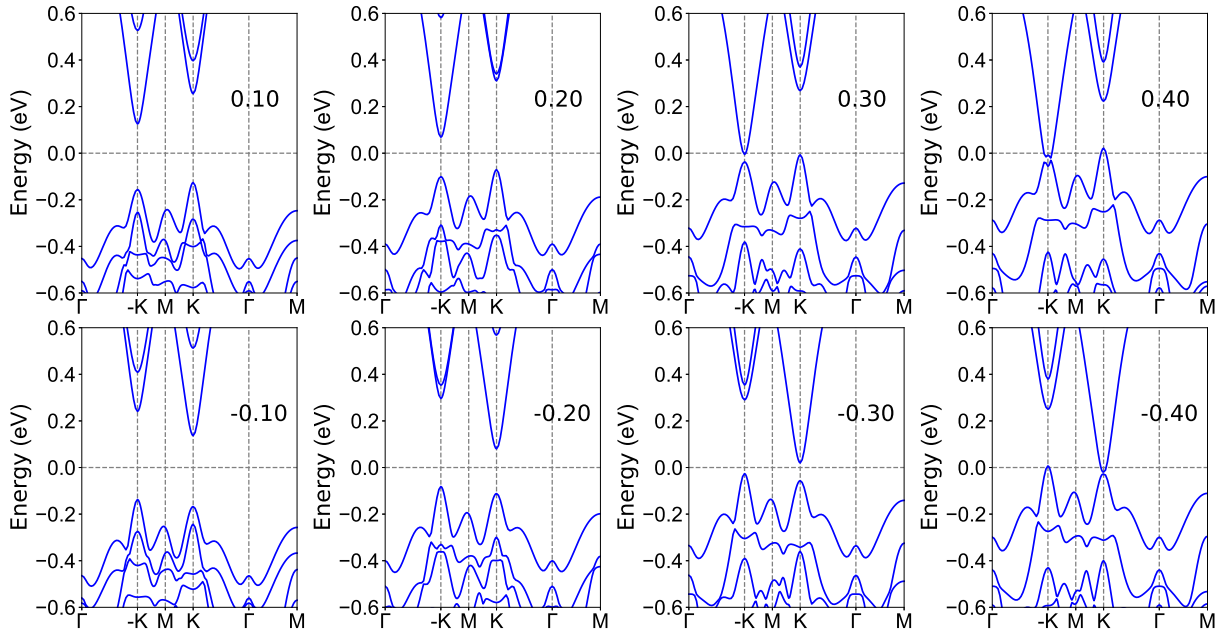


FIG. 5. (Color online) The energy band structures of AB-stacked bilayer RuBr<sub>2</sub> at representative  $E = \pm 0.10, \pm 0.20, \pm 0.30$  and  $\pm 0.40$  V/Å.

ferromagnetic (FM) ordering can give rise to ferrovalley features. The RuBr<sub>2</sub> shows a spontaneous valley splitting of 265 (31) meV in the conduction (valence) band edge at  $U = 2.5$  eV<sup>26</sup>. Here, we only construct AB-stacked bilayer RuBr<sub>2</sub>, which is plotted in FIG.1 of electronic supplementary information (ESI). The BA-stacked bilayer has the same results with AB-stacked case, when the electric field and sign of valley polarization are simultaneously reversed.

The bilayer RuBr<sub>2</sub> has the space group of  $P3m1$ , whose inversion symmetry and horizontal mirror symmetry are broken. The optimized lattice constant of bilayer RuBr<sub>2</sub> is 3.72 Å, and the interlayer distance is 3.16 Å. The AB and BA cases are energetically degenerate with opposite electric polarizations, and connect each other by interlayer sliding<sup>31</sup>. The spontaneous out-of-plane electric polarization is along positive  $z$  direction in the AB-stacked bilayer. To determine the ground state of bilayer RuBr<sub>2</sub>, the intralayer FM and interlayer FM, and intralayer FM and interlayer antiferromagnetic (AFM) magnetic configurations are considered. Calculated results show that bilayer RuBr<sub>2</sub> prefers A-type antiferromagnetism (intralayer FM and interlayer AFM orderings). This A-type antiferromagnetism is 7.4 meV per Ru atom lower than that with the FM interlayer exchange interaction.

The energy band structures of AB case are plotted in Figure 4 along with layer- and Ru- $d$ -orbital characters ones. The AB bilayer shows an indirect band gap of 0.373 eV, and the VBM and CBM locate at the K and -K points, respectively. It is clearly seen that the VBM (CBM) is from the dn-(up-)layer (Figure 4 (b)), and the valleys are layer-locked with spontaneous valley

polarization. The valley splitting in the valence (conduction) bands are defined as:  $\Delta E_V = E_V^K - E_V^{-K}$  ( $\Delta E_C = E_C^K - E_C^{-K}$ ), and the calculated value is 4.8 meV (8.10 meV). According to Figure 4 (c), it is found that the valley splitting of conduction band of monolayer RuBr<sub>2</sub> is observable, while the valley splitting of valence band is very small, which is due to different distribution of Ru- $d$  orbitals. The valley splitting  $|\Delta E|$  can be expressed as<sup>43,44</sup>:  $|\Delta E| = |E^K - E^{-K}| = 4\alpha$  ( $\alpha$  is the SOC-related constant), when  $d_{x^2-y^2} + d_{xy}$  orbitals dominate the K and -K valleys. If the -K and K valleys are mainly from  $d_{z^2}$  orbitals, the valley splitting  $|\Delta E|$  will become:  $|\Delta E| = |E^K - E^{-K}| \approx 0$ .

Essentially, ferroelectricity polarization and electric field are equivalent to produce valley polarization in valleytronic bilayer. Here, the electric field effects on valley polarization in bilayer RuBr<sub>2</sub> are investigated. Firstly, we determine the magnetic ground state under the positive and negative electric field, and the energy differences (per Ru atom) between interlayer FM and AFM ordering as a function of electric field  $E$  are shown in FIG.2 of ESI. Calculated results show that the interlayer AFM state is always ground state within considered  $E$  range, and applied electric field can enhance the interlayer AFM interaction.

The energy band structures of bilayer RuBr<sub>2</sub> under representative electric field  $E$  are plotted in Figure 5, and the evolutions of related energy band gap and the valley splitting for both valence and conduction bands as a function of  $E$  are plotted in Figure 6. For increasing positive  $E$ , the global gap decreases, and a semiconductor to metal transition is induced at  $E = 0.30$  V/Å. By applying

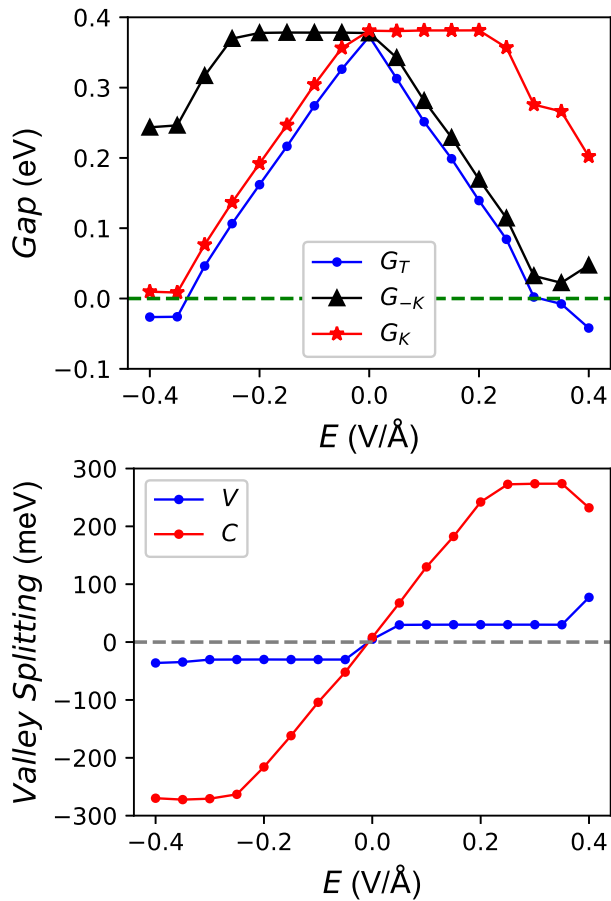


FIG. 6. (Color online) The related band gaps (top panel) and valley splitting for both valence and conduction bands (bottom panel) of AB-stacked bilayer RuBr<sub>2</sub> as a function of  $E$ .

positive  $E$ , the energy band from dn-layer is shifted toward high energy with respect to one of up-layer. When increasing positive  $E$ , the energy levels at K valley from different layers in the conduction bands near Fermi level will coincide at about  $E=0.20$  V/Å. For  $E>0.20$  V/Å, the -K and K valleys of bilayer system in the conduction bands are from the same up-layer, which can be clearly seen from FIG.3 of ESI (for example  $E=0.40$  V/Å). For the valence bands, these phenomena can also be observed, and the critical  $E$  is very small, which is due to small valley splitting in the valence bands for monolayer RuBr<sub>2</sub> at  $U=2.5$  eV. With increasing positive  $E$ , the gap of K valley firstly remains almost unchanged, and then decreases. However, for the gap of -K valley, it decreases, and then increases at about  $E=0.35$  V/Å. For  $0$  V/Å  $< E < 0.25$  V/Å, the valley splitting in the conduction bands increases with increasing positive  $E$ . At  $E=0.25$  V/Å, the valley splitting of conduction bands reaches up to 273 meV, which is close to one (265 meV) of monolayer RuBr<sub>2</sub><sup>26</sup>. The analysis above can also be applied to negative  $E$  case. The difference mainly includes two aspects: (1) the K and -K valleys exchange each other; (2) the negative  $E$  firstly need to cancel out

the small polarized electric field. When an appropriate positive electric field is reversed, the sign of valley polarization can also be reversed.

Figure 7 present the calculated Berry curvatures  $\Omega(k)$  of bilayer RuBr<sub>2</sub> under  $E=\pm 0.10$  V/Å. The valley splitting for the conduction (valence) band is 130 (30.0) meV and 104 (30.2) meV for  $+0.10$  V/Å and  $-0.10$  V/Å, which are larger than one (8.1 meV (4.8 meV)) without applying  $E$ . For  $+0.10$  V/Å case, the energy of K valley is higher than one of -K valley. The valley polarization can be switched by reversing the electric field direction from  $+z$  to  $-z$  direction. For the two situations, we observe opposite signs of Berry curvature around -K and K valleys with the unequal magnitudes. By reversing the electric field, the magnitudes of Berry curvature at -K and K valleys exchange each other, but their signs remain unchanged.

Under an in-plane longitudinal  $E$ , Bloch electrons at K and -K valleys will obtain anomalous velocity:  $v \sim E \times \Omega(k)$ <sup>45</sup>. An appropriate doping makes the Fermi level fall between the -K and K valleys. With applied in-plane and out-of-plane electric fields, the Berry curvature forces the carriers to accumulate on one side of one layer of bilayer. When the out-of-plane electric field is reversed, the carriers accumulate on one side of the other layer of bilayer. These give rise to LP-AVH effect.

The concepts of FVS and HVM have been proposed, which can achieve spontaneous valley polarization<sup>13,14</sup>. For FVS, the K and -K valleys are both insulating (Figure 1 (a)). For HVM, one of K and -K valleys is insulating, while the other is metallic (Figure 1 (b)). The HVM can be realized by changing electron correlation strength or applying strain, which is just at one point, not a region of electron correlation strength or strain. Recently, the QHVM is proposed (Figure 1 (c)), where electron and hole carriers simultaneously exist with only a type of carrier being valley polarized (The Fermi level slightly touches CBM and VBM, and the carriers around  $\Gamma$  possess almost zero Berry curvatures.)<sup>29</sup>. Here, the FVM is proposed (Figure 1 (d)), where the K and -K valleys are both metallic. For FVM, electron and hole carriers simultaneously exist, and the Fermi level slightly touches CBM and VBM. Under an in-plane longitudinal  $E$ , the Berry curvature forces the electron carriers to accumulate on one side of sample, and hole ones to move toward the other side. In the bilayer RuBr<sub>2</sub>, the FVM can be achieved by applying electric field. At  $E=0.40$  V/Å, the Fermi level slightly touches the -K valley of conduction bands and K valley of valence bands, which are from different layer (FIG.3 of ESI). The gaps of -K and K valleys are 47 meV and 202 meV, respectively. Under an in-plane longitudinal  $E$ , the electron and hole carriers accumulate on one side of different layer. In the extreme case, the Fermi level touches the valley bottom of -K valley of conduction bands and the valley top of K valley of valence bands (Figure 5 at  $E=0.30$  V/Å), which can achieve VGS-2 (Figure 2 (d)).

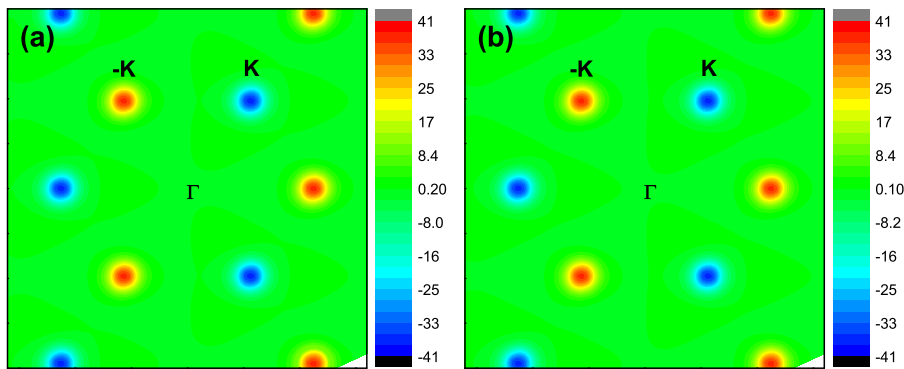


FIG. 7. (Color online) The Berry curvatures of AB-stacked bilayer RuBr<sub>2</sub> in BZ at representative  $E=0.10$  V/Å (a) and  $-0.10$  V/Å (b).

#### IV. DISCUSSION AND CONCLUSION

For monolayer FVS with hexagonal symmetry, the spontaneous valley polarization depends on the magnetization direction<sup>15-27</sup>. For out-of-plane magnetization, the monolayer FVS possess spontaneous valley polarization. However, for in-plane magnetization, no spontaneous valley polarization can be produced. For bilayer system from parent monolayer with in-plane magnetization, the K and -K valleys are from the same layer. By applying an out-of-plane electric polarization or external electric field, the bilayer system has not spontaneous valley polarization. To confirm this, layer-characters energy band structures at  $E=\pm 0.15$  V/Å are plotted in FIG.4 of ESI with in-plane magnetization. It is clearly seen that the K and -K valleys of both valence and conduction bands are from the same layer, and no spontaneous valley polarization can be observed.

To determine magnetization direction, we calculate the MAE of bilayer RuBr<sub>2</sub>, which is defined as the energy difference with the magnetization axis along in-plane and out-of-plane directions. The MAE as a function of  $E$  is plotted in FIG.5 of ESI, which indicates that bilayer RuBr<sub>2</sub> favor in-plane magnetization orientation within considered  $E$  range due to negative MAE. Therefore, bilayer RuBr<sub>2</sub> intrinsically has no spontaneous valley polarization at  $U=2.5$  eV. The previous work shows that the magnetic anisotropy direction of monolayer RuBr<sub>2</sub> changes from out-of-plane to in-plane one with the critical  $U$  value of 2.07 eV<sup>26</sup>. If the real  $U$  falls in the range ( $U < 2.07$  eV), bilayer RuBr<sub>2</sub> will possess spontaneous valley polarization.

Even though the real  $U$  falls outside the range, the spontaneous valley polarization can be achieved by strain. By applying strain, the bandwidth can be modified, which effectively controls the relative importance of electronic correlation. To reduce relative importance of electronic correlation, the compressive strain should

be used, which equivalently reduces  $U$  value. To demonstrate this point,  $a/a_0=0.95$  biaxial strain is applied on the bilayer RuBr<sub>2</sub> with  $U=2.5$  eV. Calculated results show that strained bilayer RuBr<sub>2</sub> prefers A-type antiferromagnetism, which is 9.8 meV per Ru atom lower than that with the FM interlayer exchange interaction. The calculated MAE is 909  $\mu\text{eV}/\text{Ru}$ , which indicates that strained bilayer RuBr<sub>2</sub> favor out-of-plane magnetization orientation. The energy band structures of bilayer RuBr<sub>2</sub> is plotted in FIG.6 of ESI, and the valley splitting in the valence (conduction) bands is -14.6 meV (-3.0 meV).

In summary, we have demonstrated that the electric field can effectively tune valley properties of bilayer RuBr<sub>2</sub>. The FVM and VGS-2 can be realized in bilayer RuBr<sub>2</sub> by electric field tuning. In addition, the electric field can enhance the valley splitting of bilayer RuBr<sub>2</sub>, and make the -K and K valleys be from the same layer. We take bilayer RuBr<sub>2</sub> as a concrete example, but the analysis here can be readily extended to other valleytronic van der Waals bilayers. Our findings can expand understanding of valleytronic van der Waals bilayers, and realize new valleytronic materials: FVM and VGS-2.

#### SUPPLEMENTARY MATERIAL

See the supplementary material for crystal structures; energy difference between FM and AFM and MAE as a function of  $E$ ; the related energy band structures.

#### Conflicts of interest

There are no conflicts to declare.

#### ACKNOWLEDGMENTS

This work is supported by Natural Science Basis Research Plan in Shaanxi Province of China (2021JM-456). We are grateful to Shanxi Supercomputing Center of China, and the calculations were performed on TianHe-2.

- 
- <sup>1</sup> X. Xu, W. Yao, D. Xiao, and T. F. Heinz, *Nat. Phys.* **10**, 343 (2014).
- <sup>2</sup> Y. Liu, C.-S. Lian, Y. Li, Y. Xu, and W. Duan, *Phys. Rev. Lett.* **119**, 255901 (2017).
- <sup>3</sup> M. Zeng, Y. Xiao, J. Liu, K. Yang and L. Fu, *Chem. Rev.* **118**, 6236 (2018).
- <sup>4</sup> K. F. Mak, K. He, J. Shan, and T. F. Heinz, *Nat. Nanotechnol.* **7**, 494 (2012).
- <sup>5</sup> D. MacNeill, C. Heikes, K. F. Mak, Z. Anderson, A. Kormányos, V. Zólyomi, J. Park and D. C. Ralph, *Phys. Rev. Lett.* **114**, 037401 (2015).
- <sup>6</sup> H. Zeng, J. Dai, W. Yao, D. Xiao and X. Cui, *Nat. Nanotechnol.* **7**, 490 (2012).
- <sup>7</sup> A. Srivastava, M. Sidler, A. V. Allain, D. S. Lembke, A. Kis, and A. Imamoglu, *Nat. Phys.* **11**, 141 (2015).
- <sup>8</sup> C. Zhao, T. Norden, P. Zhang, P. Zhao, Y. Cheng, F. Sun, J. P. Parry, P. Taheri, J. Wang, Y. Yang, T. Scrace, K. Kang, S. Yang, G. Miao, R. Sabirianov, G. Kioseoglou, W. Huang, A. Petrou and H. Zeng, *Nat. Nanotechnol.* **12**, 757 (2017).
- <sup>9</sup> H. Zeng, J. Dai, W. Yao, D. Xiao, and X. Cui, *Nat. Nanotechnol.* **7**, 490 (2012).
- <sup>10</sup> J. R. Schaibley, H. Yu, G. Clark, P. Rivera, J. S. Ross, K. L. Seyler, W. Yao, and X. Xu, *Nat. Rev. Mater.* **1**, 16055 (2016).
- <sup>11</sup> M. S. Mrudul, Á. Jiménez-Galán, M. Ivanov and G. Dixit, *Optica* **8**, 422 (2021).
- <sup>12</sup> M. S. Mrudul and G. Dixit, *J. Phys. B* **54**, 224001 (2021).
- <sup>13</sup> W. Y. Tong, S. J. Gong, X. Wan, and C. G. Duan, *Nat. Commun.* **7**, 13612 (2016).
- <sup>14</sup> H. Hu, W. Y. Tong, Y. H. Shen, X. Wan, and C. G. Duan, *npj Comput. Mater.* **6**, 129 (2020).
- <sup>15</sup> S. D. Guo, J. X. Zhu, W. Q. Mu and B. G. Liu, *Phys. Rev. B* **104**, 224428 (2021).
- <sup>16</sup> X. Y. Feng, X. L. Xu, Z. L. He, R. Peng, Y. Dai, B. B. Huang and Y. D. Ma, *Phys. Rev. B* **104**, 075421 (2021).
- <sup>17</sup> Q. R. Cui, Y. M. Zhu, J. H. Liang, P. Cui and H. X. Yang, *Phys. Rev. B* **103**, 085421 (2021).
- <sup>18</sup> X. Zhou, R. Zhang, Z. Zhang, W. Feng, Y. Mokrousov and Y. Yao, *npj Comput. Mater.* **7**, 160 (2021).
- <sup>19</sup> H. X. Cheng, J. Zhou, W. Ji, Y. N. Zhang and Y. P. Feng, *Phys. Rev. B* **103**, 125121 (2021).
- <sup>20</sup> R. Li, J. W. Jiang, W. B. Mi and H. L. Bai, *Nanoscale* **13**, 14807 (2021).
- <sup>21</sup> K. Sheng, Q. Chen, H. K. Yuan and Z. Y. Wang, *Phys. Rev. B* **105**, 075304 (2022).
- <sup>22</sup> P. Jiang, L. L. Kang, Y. L. Li, X. H. Zheng, Z. Zeng and S. Sanvito, *Phys. Rev. B* **104**, 035430 (2021).
- <sup>23</sup> R. Peng, Y. Ma, X. Xu, Z. He, B. Huang, and Y. Dai, *Phys. Rev. B* **102**, 035412 (2020).
- <sup>24</sup> K. Sheng, B. K. Zhang, H. K. Yuan and Z. Y. Wang, *Phys. Rev. B* **105**, 195312 (2022).
- <sup>25</sup> S. D. Guo, J. X. Zhu, M. Y. Yin and B. G. Liu, *Phys. Rev. B* **105**, 104416 (2022).
- <sup>26</sup> S. D. Guo, W. Q. Mu and B. G. Liu, *2D Mater.* **9**, 035011 (2022).
- <sup>27</sup> H. Huan, Y. Xue, B. Zhao, G. Y. Gao, H. R. Bao and Z. Q. Yang, *Phys. Rev. B* **104**, 165427 (2021).
- <sup>28</sup> S. D. Guo, Y. L. Tao, W. Q. Mu and B. G. Liu, *Front. Phys.* **18**, 33304 (2023).
- <sup>29</sup> S. D. Guo, Y. L. Tao, Z. Y. Zhao, B. Wang, G. Z. Wang, X. T. Wang, arXiv:2210.11827 (2022).
- <sup>30</sup> X. L. Wang, *Phys. Rev. Lett.* **100**, 156404 (2008).
- <sup>31</sup> T. Zhang, X. L. Xu, B. B. Huang, Y. Dai, L. Z. Kou and Y. D. Ma, *Mater. Horiz.* (2022), <https://doi.org/10.1039/D2MH00906D>
- <sup>32</sup> A. O. Fumega and J. L. Lado, arXiv:2209.09669 (2022).
- <sup>33</sup> P. Hohenberg and W. Kohn, *Phys. Rev.* **136**, B864 (1964); W. Kohn and L. J. Sham, *Phys. Rev.* **140**, A1133 (1965).
- <sup>34</sup> G. Kresse, *J. Non-Cryst. Solids* **193**, 222 (1995).
- <sup>35</sup> G. Kresse and J. Furthmüller, *Comput. Mater. Sci.* **6**, **15** (1996).
- <sup>36</sup> G. Kresse and D. Joubert, *Phys. Rev. B* **59**, 1758 (1999).
- <sup>37</sup> J. P. Perdew, K. Burke and M. Ernzerhof, *Phys. Rev. Lett.* **77**, 3865 (1996).
- <sup>38</sup> S. L. Dudarev, G. A. Botton, S. Y. Savrasov, C. J. Humphreys and A. P. Sutton, *Phys. Rev. B* **57**, 1505 (1998).
- <sup>39</sup> S. Grimme, S. Ehrlich and L. Goerigk, *J. Comput. Chem.* **32**, 1456 (2011).
- <sup>40</sup> T. Fukui, Y. Hatsugai and H. Suzuki, *J. Phys. Soc. Japan.* **74**, 1674 (2005).
- <sup>41</sup> H. J. Kim, <https://github.com/Infant83/VASPBERRY>, (2018).
- <sup>42</sup> H. J. Kim, C. Li, J. Feng, J.-H. Cho, and Z. Zhang, *Phys. Rev. B* **93**, 041404(R) (2016).
- <sup>43</sup> P. Zhao, Y. Dai, H. Wang, B. B. Huang and Y. D. Ma, *ChemPhysMater*, **1**, 56 (2022).
- <sup>44</sup> R. Li, J. W. Jiang, W. B. Mi and H. L. Bai, *Nanoscale* **13**, 14807 (2021).
- <sup>45</sup> D. Xiao, M. C. Chang, and Q. Niu, *Rev. Mod. Phys.* **82**, 1959 (2010).